Coupled Multifield Analysis of Piezoelectrically Actuated Microfluidic Device for Transdermal Drug Delivery Applications

Muhammad Waseem Ashraf, Shahzadi Tayyaba, Nitin Afzulpurkar, Asim Nisar, Adisorn
Tuantranont, and Erik L J Bohez

Abstract—In this paper, design, fabrication and coupled multifield analysis of hollow out-of-plane silicon microneedle array with piezoelectrically actuated microfluidic device for transdermal drug delivery (TDD) applications is presented. The fabrication process of silicon microneedle array is first done by series of combined isotropic and anisotropic etching processes using inductively coupled plasma (ICP) etching technology. Then coupled multifield analysis of MEMS based piezoelectrically actuated device with integrated 2×2 silicon microneedle array is presented. To predict the stress distribution and model fluid flow in coupled field analysis, finite element (FE) and computational fluid dynamic (CFD) analysis using ANSYS rather than analytical systems has been performed. Static analysis and transient CFD analysis were performed to predict the fluid flow through the microneedle array. The inlet pressure from 10 kPa to 150 kPa was considered for static CFD analysis. In the lumen region fluid flow rate 3.2946 µL/min is obtained at 150 V for 2×2 microneedle array. In the present study the authors have performed simulation of structural, piezoelectric and CFD analysis on three dimensional model of the piezoelectrically actuated mcirofluidic device integrated with 2×2 microneedle array.

Keywords—Coupled multifield, finite element analysis, hollow silicon microneedle, transdermal drug delivery.

I. INTRODUCTION

TRANSDERMAL drug delivery (TDD) is an alternative way to transport certain drugs which cannot be ideally delivered by hypodermal injections and oral methods. Transdermal drug delivery refers to the movement of pharmaceutical compounds across the skin to reach the systemic circulation for subsequent distribution in the human body. Various chemical enhancers, electroporation and physical enhancers have been proposed to promote the transdermal drug delivery [1], [2]. Microneedles are effectively used to painlessly deliver the big molecules into subcutaneous tissue with the rate at therapy level.

M. W. Ashraf (Phone: +66873516061; Fax: +66 02 524 5697; e.mail: (Muhammad.Waseem.Ashraf@ait.ac.th), S. Tayyaba (shahzadi_tayyaba @ait.ac.th), N. Afzupurkar (nitin@ait.ac.th), A. Nisar (Asim.Nisar@ait.ac.th), Erik LJ Bohez (Bohez@ait.ac.th) are with School of Engineering and Technology, Asian Institute of Technology (AIT), P.O. Box 4, Klong Luang, Pathumthani, 12120, Thailand.
A. Tuantranont (adisorn.tuantranont@nectec.or.th) is with Nanoelectronics and MEMS Lab, National Electronics and Computer Technology Center (NECTEC), Thailand.

Microneedles with lumen and reservoir were developed for local delivery with précise dose and controlled release [3]. The idea of using miconeedles for drug delivery on skin was presented in 1976 by Alza Corporation [4], but it was not displayed experimentally until 1990s when the industry of microelectronics provided the microfabrication tools essential to make such small structures. Hollow microneedles are used to deliver the drugs through a microfluidic system, or coated with drugs which release after insertion into the skin [5]. Side opened out-of-plane microneedles were fabricated for microfluidic transdermal liquid transfer [6]. The microneedle arrays, integrated with fluidic microchannels are used for extraction and analysis of biofluids from just beneath the skin surface, using only capillary actions [7]. Silicon microneedle electrode arrays were fabricated for electroporation [8]. Fabrication of microneedle arrays was reported for microdialysis [9]. Various microfluidic devices integrated with microneedle array have been reported in literature for transdermal drug delivery applications [10], [11]. Microneedle designs vary in needle geometry, array density and materials. The microneedles are classified as in-plane and out-of-plane microneedles based on the fabrication process. A schematic illustration of in-plane and out-of-plane microneedles is shown in Fig.1. In in-plane microneedles, the microneedle shaft is parallel to the substrate surface. In out-of-plane microneedles, the length of the microneedles protrudes out of the substrate surface.
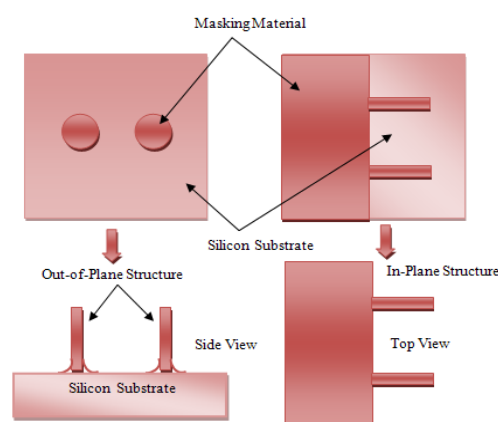

Fig. 1 In-plane and out-of-plane microneedles structure
Out-of-plane microneedles are easier to fabricate in arrays.

World Academy of Science, Engineering and Technology
International Journal of Electronics and Communication Engineering
Vol:4, No:2, 2010

According to the geometry, the microneedles can be solid or hollow. In hollow microneedles, an internal lumen is present which allows fluid flow through the microneedles. Microneedle arrays based devices currently find their way into many applications in biomedical. In this paper, the design, fabrication of hollow out-of-plane silicon microneedle array and numerical analysis of silicon microneedle array based piezoelectrically actuated microfluidic device is presented.

II. FABRICATION

The proposed microneedle array fabrication process with integrated drug reservoir involves isotropic and anisotropic etching processes using standard silicon wafers. The desired shape of microneedle array structures was achieved by controlling the etching process at various processing steps. The fabrication process involves many steps with each step having many substeps. The steps of fabrication process are shown in Fig. 2. The single sided polished six inch silicon wafer is first cleaned with Piranha solution and DI water and dried. After cleaning, caping of photoresist mask is done. This step involves various substeps such as spin coating photoresist AZ4620 @3000 rpm, soft bake (120-180 sec @ 110° C), expose wafer, develop in developer solution AZ 400K and hard bake. Then isotropic silicon dry etching of silicon wafer with ICP etch tool is done using SF_6/O_2 gases for outside shape of microneedle tips in standard photolithography process (Etch Depth = 15μm).

PR coat/Soft bake/Expose/Develop/Hard bake

15μm (SF_6 etch depth) Strip Photo resist

Thermal Oxidation (2μm)

Back side mask oxide etch

Front side mask oxide etch

Coat Photo resists (5μm)

First ICP Etch (Depth 150 μm)

Second ICP Etch (Depth 200 μm)

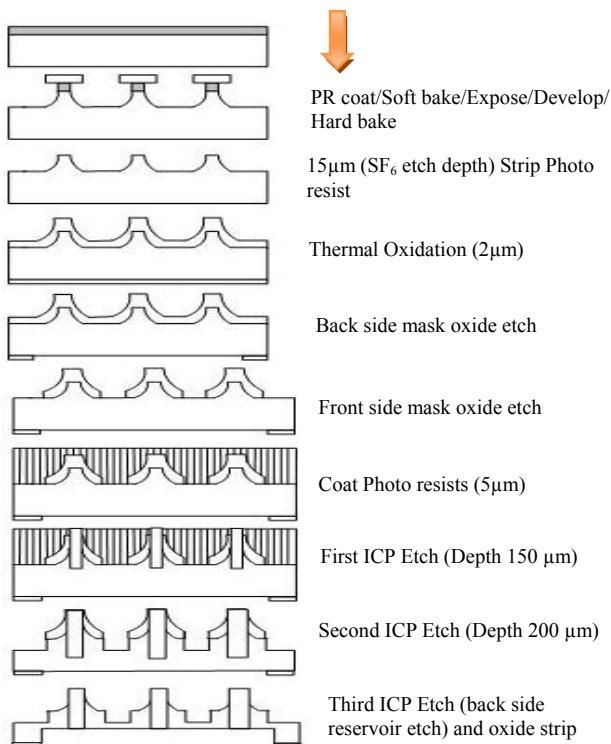Third ICP Etch (back side reservoir etch) and oxide strip

Fig. 2 Fabrication process out-of-plane silicon microneedles

Then photoresist is stripped off and wafer is cleaned. Then silicon oxide layer (2 μm thickness) is grown thermally on both sides of the wafer in oxidation furnace by wet oxidation at 1000° C. Then each side of wafer is protected by capping with another wafer for mask oxide etching. Then photoresist is stripped. To perform first ICP etching, the photoresist is first coated with 5 μm thickness. The etching depth for first ICP etch is 150 μm. This is followed by second ICP etch up to 200 μm for backside reservoir etching. The front side is then capped and third ICP etching is done to make the reservoir on the backside of the wafer. The final steps involve release, oxide etch and dicing. The SEM image of fabricated microneedle array is shown by the Fig. 3. The microneedle tip was fabricated by isotropic etching using SF_6/O_2 gases in inductively coupled plasma etcher. The outside vertical shape, lumen etching and back side etching were done using the BOSCH process. Using above process the microneedles, with dimension designs (I.D. = 40 μm, O.D. = 425 μm center-to-center spacing = 750 μm) were fabricated successfully.
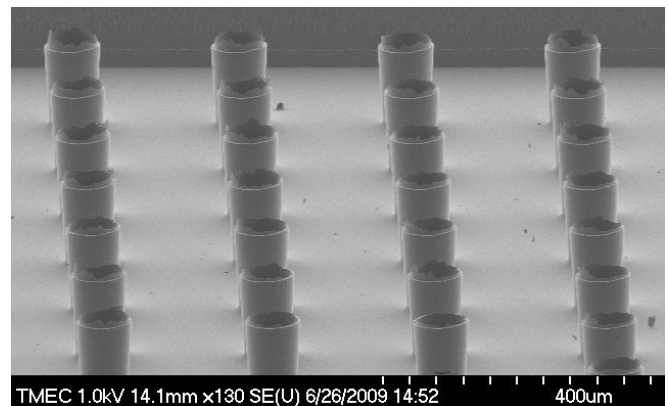
Fig. 3 SEM image of fabricated hollow microneedle array

III. MICRONEEDLE MECHANICS

The microneedle experiences resistive force exerted by skin during insertion, hence in order to pierce the microneedle into the skin, the applied axial force should be greater than the skin resistance force. An axial force acts on the microneedle tip during insertion. This axial force is compressive and causes buckling of the microneedle. Failure of microneedle is possible during skin insertion due to bending or buckling. The axial force can be reduced by decreasing the tip area of the microneedle. As buckling is directly related with compressive force, which acts during insertion, sharp microneedle tip reduces buckling. Hence insertion of microneedle into the skin becomes easy. On the other hand, bending may occur due to uneven skin surface or human error during needle insertion. Therefore, it is important to find the relation between microneedle geometry and mechanical properties of the material for proper microneedle design and to predict failure of the microneedle. The axial force (compressive force) which the microneedle can withstand without breaking is given by (1).

$$F_{Compressive} = \sigma_y A \qquad (1)$$

World Academy of Science, Engineering and Technology
International Journal of Electronics and Communication Engineering
Vol:4, No:2, 2010

Where, σ_y is yield stress, and A is cross sectional area of the microneedle tip which is very small.

The buckling force acting on the hollow microneedle during insertion is given by (2) [12], [13].

$$F_{Buckling} = \frac{\pi^2 EI}{L^2} \qquad (2)$$

Where, E is young's modulus, I is moment of inertia, and L is length of the microneedle.

The bending force at which the microneedle can withstand without breaking is given by (3).

$$F_{Bending} = \frac{\sigma_y I}{cL} \qquad (3)$$

Where, $c = D/2$ is the distance from vertical axis to the outer edge of the section.

IV. MICROFLUIDIC ANALYSIS

Fluid flow characteristics are extremely important because array of microneedle is used to inject drug solutions into human skin. The pressure drop required in the microneedles for fluid is based on various factors such as microneedles geometry, fluid viscosity, roughness of surface and microneedles density. Equation 4 shows the Poiseulle's law of fluid flow in a cylinder that is considered to determine fluid flow through array of microneedle.

$$Q = \frac{\pi d^4 (\nabla P)}{128 \mu (L)} \qquad (4)$$

Where, Q is flow rate, d is inner diameter of the microneedle, ∇P is pressure drop across the microneedle lumen, μ is viscosity of fluid for water at 25 ^{0}C, and L is length of lumen of the microneedle.

Bernoulli equation is shown in (5). This equation is considered to model the microneedles geometry. The pressure loss is calculated by considering the friction losses [14], [15].

$$\frac{P_1}{\rho g} + \frac{V_1}{2g} + Z_1 = \frac{P_2}{\rho g} + \frac{V_2}{2g} + Z_2 + \frac{fL}{d}\frac{V^2}{2g} + \Sigma \frac{KV^2}{2g} \qquad (5)$$

Where, P_1 is inlet pressure, P_2 is outlet pressure, V_1 is inlet velocity, V_2 is outlet velocity, ρ is density of water, z_1 and z_2 are distances, and f is friction factor.

V. CFD ANALYSIS

CFD analysis of piezoelectrically actuated microfluidic device with integrated 2×2 microneedle array was conducted to predict the flow rate and pressure drop of the fluid flowing through the microneedle. CFD analysis is done by using two different simulations for flow rate analysis. In the first simulation, the static pressures were applied at the inlet of the reservoir. In the second type of simulation transient analysis was performed using multiple code coupling.

A. CFD Analysis at Different Inlet Pressure

In this analysis, the simulation is done by applying static pressures of 10 kPa to 150 kPa at the inlet of reservoir. For the simulation, water at 25°C was considered as fluid domain. The outlet pressure was assumed to be 0 kPa because the previous study [16] showed negligible pressure at the outlet of the microneedle. The simulation result shows that the velocity of the fluid is negligible in the reservoir zone due to large area but the velocity increases in the microneedle lumen section due to small area. Due to frictional losses between fluid and wall, the velocity of the fluid is less at the wall area of the lumen as compared to the central region of the lumen section. Simulation result of fluid flow by applying pressure of 100 kPa at inlet is shown by Fig. 4.
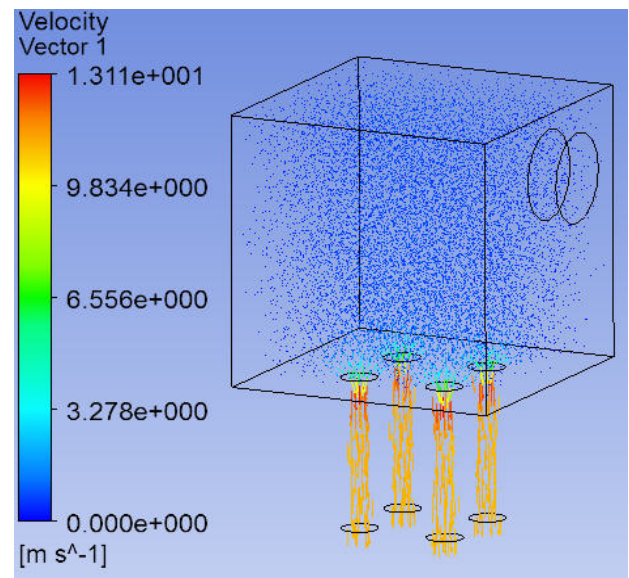

Fig. 4 Velocity variations at static pressure 100 KPa

B. CFD Analysis using Transient Multifield Code Coupling

Multifield analysis using multiple code coupling has been conducted in ANSYS for piezoelectrically actuated microfluidic device [17]. Multifield analysis involves fluid structure coupling, where structural model sends surface load to the fluid model. At the same time fluid model sends forces to the structural model during the simulation. The sequential method was used for ANSYS and CFX field analysis, where ANSYS field was solved initially. The fluid solid interface (FSI) surface is created in CFX model with same name for proper communication between ANSYS and CFX solver. Multifield simulation results were obtained using MFX-ANSYS/CFX simulation environment. The model boundary conditions for the fluid structure interface are shown in Fig. 5.

World Academy of Science, Engineering and Technology
International Journal of Electronics and Communication Engineering
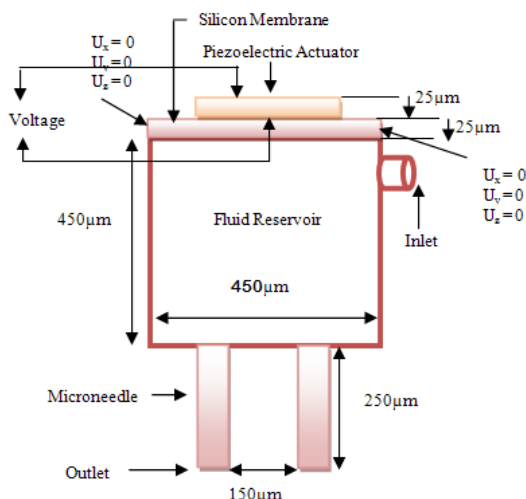Vol:4, No:2, 2010

Fig. 5 Model dimensions and boundary condition

Silicon membrane is attached to the piezoelectric actuator. The PZT4 material is used to actuate the silicon membrane. SOLID-5 element has been used for voltage degrees of freedom and SOLID-186 element has been used for the silicon membrane. Water at 25° C is used for the CFD model. The circuit element CIRCU-94 has been used for transient analysis. The thickness of the piezoelectric and silicon membrane is 50 μm. Depending on polarity of the applied voltages the silicon membrane deforms in upward and downward directions. Due to the applied voltages the periodic excitation force is generated. This force periodically deforms the silicon membrane and generates fluid flow. The analysis has involved simulation of structural, piezoelectric and CFD analysis on three dimensional model of the piezoelectrically actuated microfluidic device integrated with 2×2 microneedles array.

VI. RESULTS AND DISCUSSION

The maximum displacement in silicon membrane at 150 V occurs at the centre of the membrane that is shown in Fig. 6. The maximum deflection obtained at 150 V is 0.342 μm. The maximum Von Mises stress is observed in silicon membrane near the interface between piezoelectric layer and the silicon membrane. This stress is well below the yield strength of the silicon.
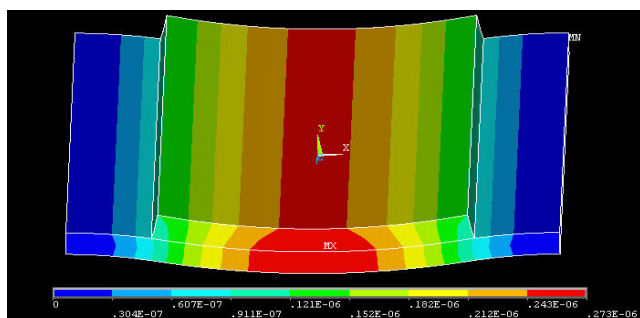

Fig. 6 Maximum displacement of silicon membrane at 120 V

The deformation of the silicon membrane at different membrane positions for various applied voltages (15V, 30V, 45V, 60V, 75V, 90V, 105V, 120V, 135V, and 150V) is shown in Fig. 7. The deformation is measured along the length of the membrane. The maximum displacement is occurred at the centre of the membrane at 225μm from the edge. The silicon membrane displacement increases with increase in the excitation voltage across the membrane.
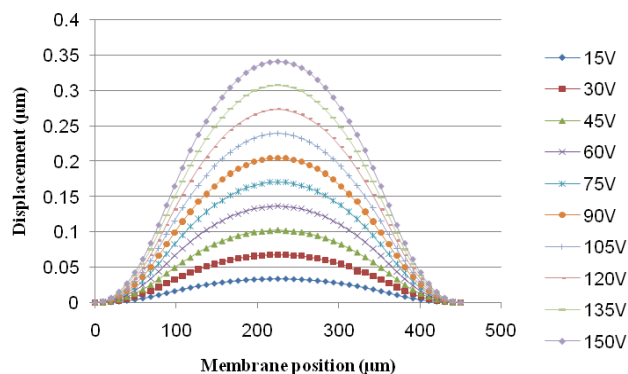

Fig.7 Membrane position Vs membrane displacement

In transient analysis, the maximum velocity due to mesh displacement at 150 V is shown in Fig. 8. The result shows that maximum velocity occurs in the lumen region due to small area. The velocity of the fluid is higher in the centre of the lumen than the wall surface due to friction between the wall and the fluid. Simulation result shows that the fluid velocity is uniform through all microneedles.
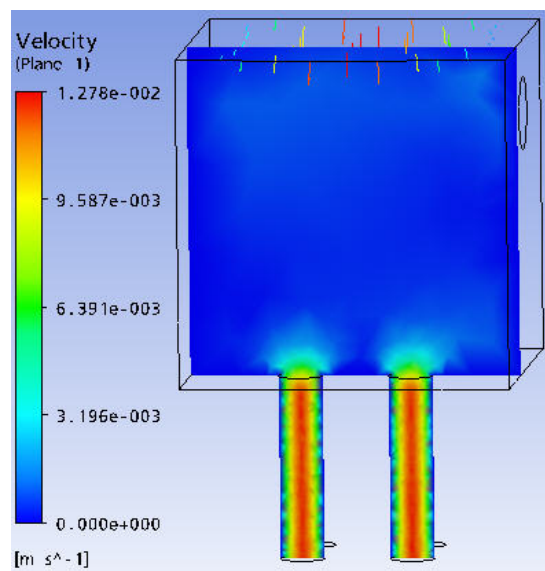

Fig. 8 Velocity variations at 150 V

The fluid velocity variations along the length of the microfluidic device for transient and static analysis are shown in Fig. 9 and Fig. 10 respectively. The fluid velocity in the reservoir is negligible due to large area. The velocity increases in lumen of the microneedles due to small area.

World Academy of Science, Engineering and Technology
International Journal of Electronics and Communication Engineering
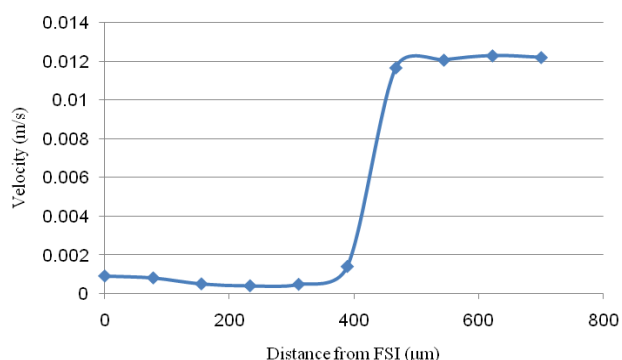Vol:4, No:2, 2010

Fig. 9 Velocity variation (transient analysis) along length of microfluidic device
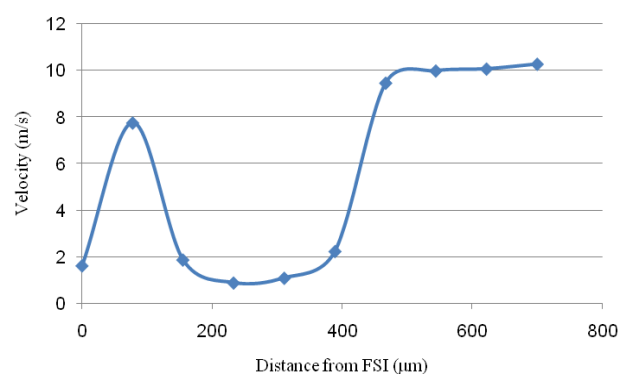

Fig. 10 Velocity variation (Static analysis) along length of microfluidic device

The maximum flow rate 3.2946 μL/min is obtained at 150 V for 2×2 microneedle array as shown in Fig. 11. Simulation results show linear response between flow rate and applied DC pulses.
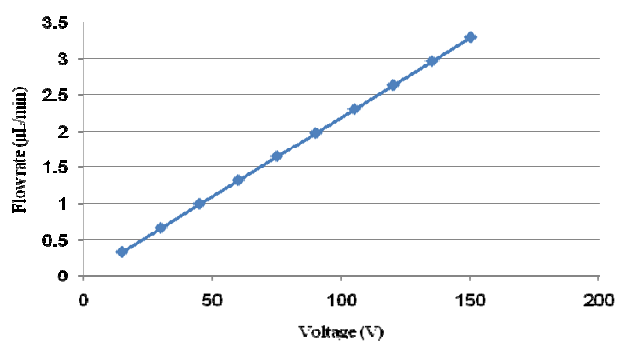

Fig. 11 Variation in flow rate at various applied voltages

VII. CONCLUSION

In this paper, fabrication of hollow out-of-plane silicon microneedles and coupled multifield analysis of microfluidic device for transdermal drug delivery applications is presented. The CFD analysis predicts uniform flow through the microneedle array for each microneedle. Using multiple code coupling fluid flow rate in the microneedle array at various applied DC pulses is numerically and theoretically calculated that are in close agreement with each other and validate the presented CFD analysis. Simulation results show that stroke volume and central displacement of silicon membrane increases with increase in excitation voltages. Minimum pressure is occurred at the outlet therefore maximum fluid flow rate is achieved at initial stroke. The presented research work provides useful information and predicted data to fabricate optimized designs of silicon hollow microneedle array based microfluidic devices for transdermal drug delivery applications.

REFERENCES

[1] B. Barry, and A. Williams, "Penetration enhancers", Adv. Drug Deliv. Rev., Vol.56, pp. 603-618, 2003.
[2] V. Preat, and R. Vanbever " Skin electroporation for Transdermal and topical delivery", ", Adv. Drug Deliv. Rev., Vol.56, pp. 659-674, 2004.
[3] Jing Ji, F. Tay. And J. Miao, "Microfabricated Hollow Microneedle Array Using ICP Etcher", *Journal of Physics, Conference series* 34, pp. 1132-136, 2006.
[4] Gerstel et al., Drug Delivery Device, US 3 964 482 patent, 1976.
[5] Mark R. Prausnitz," Microneedles for transdermal drug delivery", Adv. Drug Deliv. Rev. 56, pp. 581–587, 2004.
[6] P. Griss, and G. Stemme, "Side-opened out-of-plane microneedles for microfluidic transdermal liquid transfer", *J. Microelectromechanical Sys,* 12 (3), pp. 296–301, 2003.
[7] E.V. Mukerjee, R. Issseroff, S. D. Collins, and   R.L. Smith, "Microneedle array with integrated microchannels for transdermal sample extraction and in situ analysis", *The 12th International Conference on Solid State Sensors, Actuators and Microsystems*, pp. 1439–1441, Boston, 8–12 June 2003.
[8] N. Wilke , C. Hibert, J. O'Brien, and A. Morrissey, "Silicon microneedle electrode array with temperature monitoring for electroporation", Sensors and Actuators A 123–124, pp. 319–325, 2005.
[9] Z. Jeffrey, T. David, and L. Dorian, "Microdialysis Microneedles for Continuous Medical Monitoring", *Biomedical Microdevices* 7, pp. 59-69, 2005.
[10] M. Bin, L. Sheng, G. Zhiyin, L. Guojun, C. Xinxia, Z. Honghai, and Y. Zhigang, "A PZT insulin pump integrated with silicon microneedle array for transdermal drug delivery", *Microfluid Nanofluid* 2, pp.417-423, 2006.
[11] N. Roxhed, "A fully integrated microneedle based transdermal drug delivery system", A PhD thesis, Microsystems Technology Laboratory, Royal Institute of Technology, Sweden, 2007.
[12] J. D. Zahn, N. H. Talbot, D. Liepman, and A. P. Pisano, " microfbricated polysilicon microneedles for minimally invasive biomedical devices", *Biomed, Microdevices* 2,pp. 295-303, 2000.
[13] J. Gere, S Timoshenko, Mechanics of materials, Fourth ed., May 1997
[14] W.S. Janna," Design of fluid thermal system", 2nd edn. PWS Publications, Boston, 1998.
[15] D. W. Bodjale, A. Nisar, and N. Afzulpurkar, "structural and microfludic analysis of hollow side open polymeric microneedles for transdermal drug delivery applications", *Microfluid Nanofluid,* 2009.
[16] S. Khumpuang, R. Maeda, and S. Sugiyama, "Design and fabrication of coupled microneedle array and insertion guide array for safe penetration through skin"; *International symposium of micromechatronics and human science,* 2003.
[17] M. W. Ashraf, S. Tayyaba, A. Nisar, N. Afzulpurkar, and A. Tuantranont , "Coupledfield Microfluidic Analysis of Integrated MEMS Based Device for Transdermal Drug Delivery Applications", In: 13th IEEE Multitopic Int. Conf. Islamabad, Pakistan, December 14-15, 2009.